Combustion Modes and Reaction Paths of the Self-Sustained High-Temperature Synthesis of Intermetallic Compounds: A Computer Simulation Study of the Effect of Exothermicity

Silvia Gennari,* Filippo Maglia, Umberto Anselmi-Tamburini, and Giorgio Spinolo

INSTM, IENI/CNR, and Department Physical Chemistry, University of Pavia, Viale Taramelli, 16, I 27100 Pavia, Italy

Received: July 7, 2004; In Final Form: September 8, 2004

The effect of the thermodynamic aspects on the SHS of intermetallic compounds is investigated by computer simulation using an heterogeneous model. The exothermicity of the process is explored by changing heat of formation of the solid compound and mixing enthalpy in the liquid phase, while the kinetics is left unmodified. Different dynamic behaviors have been identified: steady propagation, pulsed propagation, extinction. Two different kinds of instabilities are shown: longitudinal instabilities and transversal instabilities. The ranges of existence of these two dynamic behaviors appear to be mutually exclusive. The occurrence of different dynamic behaviors is related to the predominant process taking place in the different cases.

1. Introduction

SHS (self-sustained high-temperature synthesis, also known as combustion synthesis) is both a powerful synthetic approach to wide classes of inorganic materials and an interesting model for dynamic systems. With this technique, an external heating pulse applied to a surface of a pellet of suitable reactant powders ignites an heterogeneous chemical reaction, which can self-sustain if "sufficiently exothermic", and then propagates in the form of a chemical and thermal wave. The experimental approach to kinetics and the mechanism of SHS process suffers from a serious lack of powerful investigation methods and of a simple and unifying analytic model.[1,2] Concerning the former, methods for directly monitoring the kinetics of the process are almost restricted to the determination of the combustion wave speed by videorecording and of the temperature profile of the external surface of the sample as a function of time, with supplementary information given by the analysis of the product at the end of the SHS, or after a thermal quenching. Recently, specific pyrometric methods have been developed,[3] and time-resolved X-ray diffraction has been successfully applied to the study of the SHS synthesis of several intermetallic compounds and composites.[4−6] Though many reduced schemes for analytical and numerical investigation of premixed and diffusion flames have recently been developed,[7−10] the need of taking into account different reaction steps, as well as the heterogeneous nature of these steps, strongly suggests a simulation approach. The idea underlying this approach is that one assumes a reaction model and a set of process parameters; then, the comparison with the time evolution of several experimental SHS runs with different process conditions is used to gain insights on the assumptions and indications for a better model.

For this purpose, the authors have developed in the last years a flexible and general numerical method[11] that is able to include several reaction steps, possibly with different kinetic laws for each of them, and models the relevant chemical kinetics at the level of the grains of the component powders. The latter feature improves the inherent deficiencies of previous models based on the theory of homogeneous premixed flames, which cannot account for the effects dependent on the sizes of the reacting solid particles, well assessed in the experimental literature.

The method has been applied to the SHS $Zr + O_2$ (g) → ZrO_2 [11−13] and to the SHS Al + Ni → AlNi.[14,15] In the first case, the simulation approach was mainly used to explore the competition between two oxidation mechanisms to show the wide range of dynamic behaviors obtained by varying partial pressure of oxygen and dilution degree of the reaction (the product itself being used as a diluent for this "very hot" reaction).[11−13] The simulation of the formation of the intermetallic compound was focused, on the contrary, on the aspects related to the heterogeneity of the process and to the need of considering many different reaction steps, as shown further on.[14,15]

In both cases, the numerical approach gives a great deal of information on various aspects of system dynamics, such as the existence of several unsteady propagation modes in addition to steady propagation, and of the routes to extinction when some SHS specific parameter is changed. Moreover, the results have been compared[16] with existing analytical and numerical results obtained using different methods.[7−10]

In a previous paper on the latter SHS,[14] it has been shown that the reaction propagates under nearly steady conditions and with a wave velocity close to experimentally reported values, when a suitable thermal conductivity of the green compact is used. Now, intermetallic systems are well-known in the SHS community as a particular case characterized by "low exothermicity" of the process, so that the amount of heat available to sustain the SHS emerges as a very significant parameter to be explored, and this exploration can be most naturally done with computer simulations. Further interest on this aspect is suggested by the theoretical approach developed by Makino[17] for SHS processes based on the reaction of a metal and a nonmetal. Particular interest relies on the existence of transversal instabilities (in addition to longitudinal instabilities) that has been recently shown also by a preliminary report from our group[16] using a 3D variant of our usual method.[11]

It is therefore the aim of the present work to give an account of the propagation dynamics of the SHS of an intermetallic

* Corresponding author. Fax: +39 0382 507575. E-mail: silvia.gennari@unipv.it.

10.1021/jp046994n CCC: $27.50
Published on Web 11/19/2004

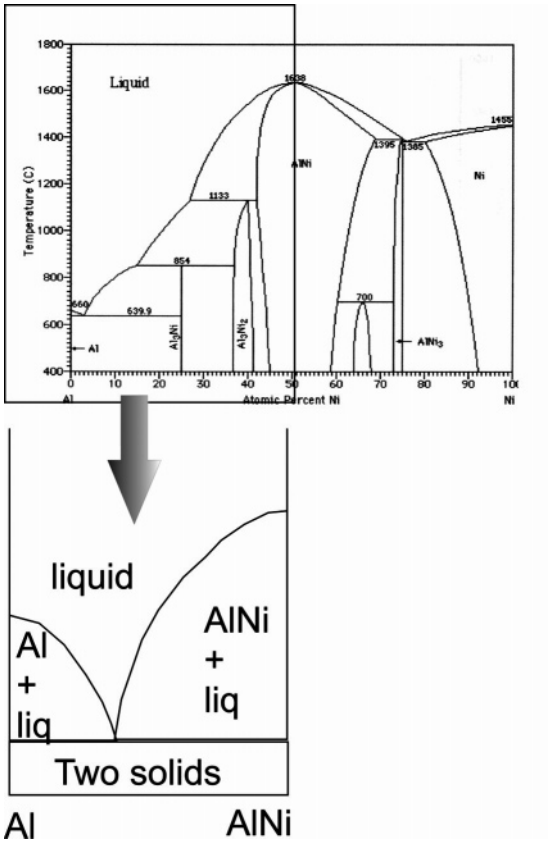

Figure 1. Outline of the experimental phase diagram of the Al−Ni system and of its simplified form in the present simulations.

compound as a function of the heat released by the various reaction steps, and to investigate the relation between the rate of these steps and the chemical reaction path actually followed by the system.

2. Thermodynamics and Computational Details

The present work is based on the Al + Ni → AlNi SHS as a reference case.

The Al/Ni system (Figure 1) actually forms five intermetallic compounds.[18,19] The 1:1 compound shows a wide homogeneity range and melts congruently at 1911 K. In the present work only this compound is taken into consideration and it is treated as a line compound. This is related to the fact that the SHS of intermetallic compounds is particularly effective when applied to the compound closer in composition to the lower melting reactant. The SHS of some other intermetallic compounds is sometimes feasible, but then the reaction mechanisms proceeds (or is believed to proceed) through previous formation of the former compound: the model here discussed is then restricted to the simplest case.

In its simplified version, the equilibrium phase diagram then shows only three biphasic areas in the composition range $0 \leq x_{Ni} \leq 0.5$ (x = mole fraction): (a) pure solid Al + liquid, (b) pure compound + liquid, and (c) pure solid Al + pure compound. It is here assumed that, when the melting temperature of the low melting metal (i.e., aluminum) is reached, this element melts and only after complete melting does the high melting metal (i.e., nickel) start to diffuse. This changes the composition of the liquid phase and moves the representative point of the system toward the biphasic (compound+ liquid) region of the phase diagram. When the system crosses the AlNi/liquidus curve, the solid compound starts precipitating as required by the phase diagram.

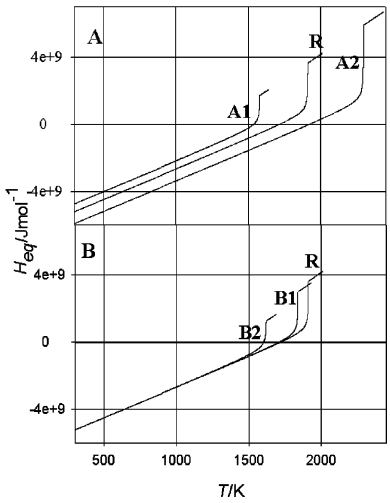

Figure 2. Equilibrium enthalpy as a function of temperature while the enthalpy of formation of the compound (A) and enthalpy of mixing (B) change. The letter R outlines the reference case ($H_0 = -53$ kJ mol^{-1} and $C_1 = -10.617$ kJ mol^{-1}), and other letters refer to the cases hereafter described.

The reaction enthalpy sustaining the SHS process actually comes from two different sources:

(a) heat of formation of the solid compound from the pure elements; the enthalpy of the compound is here modeled as $H = H_0 + C_pT$.

(b) mixing enthalpy of the liquid phase; the mixing enthalpy of this system as obtained from literature[20] follows a quasichemical model. In particular, the quasi-chemical constant is given as $K = \exp(-C_1/T + C_2)$.

The aim of the present work is to explore the exothermicity of the reaction; hence only H_0 and C_1 are changed. Moreover, it should be here noted that only realistic values of H_0 and C_1 (considering an intermetallic system) are here taken into consideration.

The reference case (from now on indicated as R) corresponds to $H_0 = -53$ kJ mol^{-1} and $C_1 = -10.617$ kJ mol^{-1}. The simulations here presented span the ranges -60 kJ mol$^{-1} \leq H_0 \leq -47$ kJ mol^{-1} and -20.617 kJ mol$^{-1} \leq C_1 \leq -5$ kJ mol^{-1}. To improve the understanding of the results, from now on four different cases will be shown in more detail: A1 refers to the system with $H_0 = -49.5$ kJ mol^{-1}, A2 refers to a system with $H_0 = -60$ kJ mol^{-1} (and the reference C_1 value), B1 shows result for a system with reference H_0 and $C_1 = -12.617$ kJ mol^{-1}, and B2 indicates a system with $C_1 = -20.617$ kJ mol^{-1} (and the reference H_0 value).

Figure 2 outlines the effect on the H/T diagram of independently changing the two enthalpy terms, and in particular shows how adiabatic temperature changes. Note that the coldest system obtained while H_0 (A1) changes corresponds to an equilibrium phase diagram similar to the hottest system obtained while C_1 (B2) changes.

The computational method[11] is based on the uncoupling of micro- and macrokinetic aspects. The former aspect models the chemical and phase transformations at the level of the grains of the reacting mixture, and the latter concerns the Fourier equation of energy transport. Technically, at each time step a chemical routine takes care of the irreversible processes at each space step and adjusts the amount and composition of the pertinent phases according to the phase diagram.

The physicochemical model has been implemented in two different ways according to the dimensionality of the problem (1D or 3D).

In our usual 1D approach[11] the simulation method basically faces the parabolic system of partial differential equations (PDE):

$$\begin{cases} C\dfrac{\partial T}{\partial t} = \nabla(\chi \nabla T) + \dfrac{2\sigma\epsilon(T^4 - T_a{}^4)}{R} + \sum_i \dot{q}^i_{\text{chem}} \\ \dot{q}^i_{\text{chem}} = f(x,y,z,T,t) \end{cases}$$

containing, in addition to Fourier's law, one or more kinetic equations. The latter ones describe, at the level of the grains of solid phases, the explicit kinetics of the assumed chemical or phase transformations. C is the heat capacity per unit volume, χ the thermal conductivity, σ the Stefan−Boltzmann constant, and ϵ the emissivity (here $\epsilon = 0.99$).

The Fourier equation has been written for a cylindrical sample of radius R and length L, and only one spatial coordinate is considered (the coordinate corresponding to the cylindrical axis). Initial and boundary conditions for Fourier equation are

$$\begin{cases} T(x,t{=}0) = T_a \;\forall\; x \in \{0,L\} \\ T(0,t) = f_1(t) \\ T(L,t) = f_2(t) \end{cases}$$

where for f_2 we usually take a constant value ($T_a = 298$ K) and f_1 is a suitable ignition function, hereafter assumed in Gaussian form, where height (maximum ignition temperature), width (time range of ignition), and position (time lag) can be indipendently set. Numerical solutions for the system have been obtained using the finite difference Crank Nicholson algorithm.

The 3D approach was implemented by linking a series of user routines to a commercial engine[21] for the solution of PDE systems based on a finite volumes (FV) scheme that directly solves a continuity equation for enthalpy. Boundary conditions and the geometrical model are the same as those for 1D (the ignition function is applied on the front face of the cylinder, while the back face and lateral surfaces are kept at room temperature).

The accuracy of the results was controlled with shorter runs with different (finer) discretisation steps in space and time. Tests were made in particular to be sure that the oscillations here obtained are real and not an artifact of the numerical algorithm. The various computational details (for 1D and 3D), as well as the FORTRAN listings, are presented in the Ph.D. Thesis of S. Gennari.[22]

The processes taken into account in chemical routines are

(a) Melting of the Al reactant: In fact, the model requires the complete melting of the low melting metal before the high melting one can start diffusing.

(b) Diffusion-controlled dissolution of solid nickel into the molten pool: This process is governed by an appropriate kinetic law,[23] and we use the invariant field approximation for the solution of the underlying diffusion equation in a semi-infinite pool following:

$$r^2 = r_0{}^2 - kDt$$

Here r is the radius of the particle at a given time, r_0 is its initial value, k depends on liquid composition at the particle−liquid interface and bulk liquid composition, and D is the diffusion coefficient given in an Arrhenius form as

$$D = D_0 \exp\left(\frac{-E_a}{RT}\right)$$

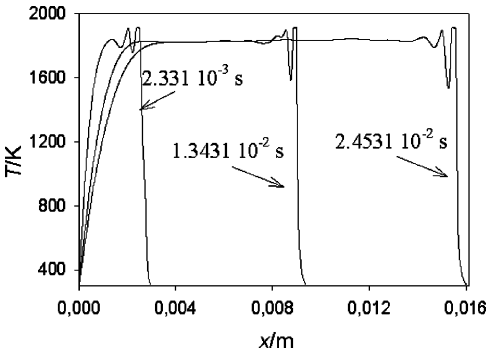

Figure 3. Space profiles of temperature at different time steps for the reference case R.

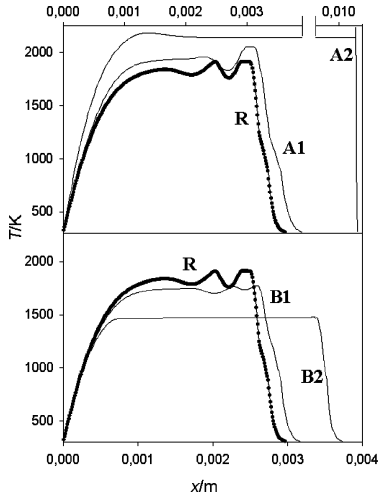

Figure 4. Temperature profiles as a function of space while the enthalpy of formation of the compound (A) and enthalpy of mixture (B) change. The starting situation R is outlined with black dots.

where $E_a = 76$ kJ mol^{-1} and $D_0 = 10^{-4}$ m^2 s^{-1} were obtained from experimental measurements in isothermal conditions.[24]

(c) Melting of the Ni reactant, when temperature overcomes the melting point of nickel.

(d) Precipitation and melting of the compound, following the phase diagram.

(e) Deposition of the eutectic mixture of Al + AlNi.

Steps a and c−e are considered without kinetics, i.e., in terms of enthalpy balance only.

In the present simulations, the radius of the cylindrical sample (R) has been fixed at 1 cm, and the initial radius of the high melting reactant particles (r_0) at 10 μm. It should be here noted that for the 3D case, explorative simulations were run while the radius of the cylinder was varied (with reference values of H_0 and C_1). Values of R of 0.2, 1, and 2 cm were used: though the morphology dependence of xy instabilities from the radius has not yet been studied in detail, changing the radius did not modify the exclusiveness of the fields of existence of longitudinal and transversal instabilities (better discussed in the following section); moreover, it did not affect the boundaries of the mode diagram reported in Figure 6.

Figure 3 shows a typical space profile of temperature at different time steps for the reference case R. The profile refers to a starting composition of 0.49 in terms of the molar fraction of nickel, to a reactant grain size of 10^{-5} m, and to bulk thermal conductivity (χ(Al,s) = 240 W m^{-1} K^{-1}, χ(Al,l) = 800 W m^{-1} K^{-1}, χ(Ni,s) = 82 W m^{-1} K^{-1}, χ(Ni,l) = 400 W m^{-1} K^{-1}, and χ(AlNi,s) = 100 W m^{-1} K^{-1}, the thermal conductivity of the heterogeneous mixture has been obtained from that of the

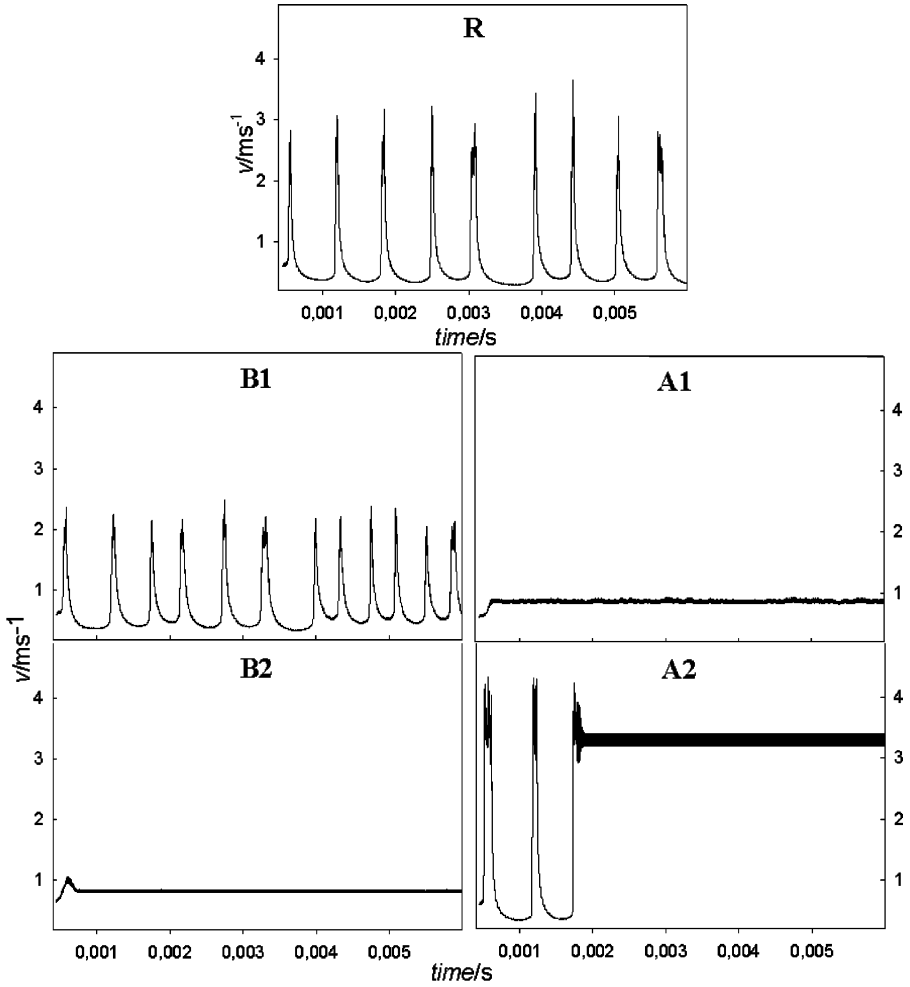

Figure 5. Propagation speed of the wave front as a function of time while the heat of formation of the solid compound (column A) and mixing enthalpy of the liquid phase (column B) change. R refers to the starting situation.

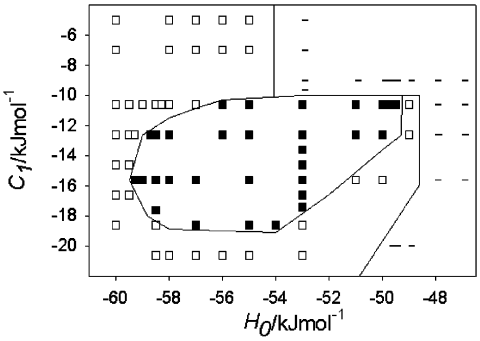

Figure 6. Dynamic behaviors for the SHS of formation of an intermetallic compound from pure elements as a function of enthalpy of formation of the compound (H_0) and enthalpy of mixture (C_1). Black dots refer to oscillating propagation modes, white dots to steady propagation, and dashes indicate systems characterized by extinction.

constituent phases by a simple linear dependence from composition). The propagation mode, as better shown in Figure 5 (R), is oscillatory and the combustion temperature is just below the melting point of the compound (≈1800 K). This situation will be taken as the starting point from which all parameters taken into consideration will be changed.

3. Results

Figure 4 shows different temperature profiles at a given time in order of increasing exothermicity. The starting situation is here outlined with dots. Plots A1 and A2 refer to the change in the formation enthalpy of the compound, and plots B1 and B2

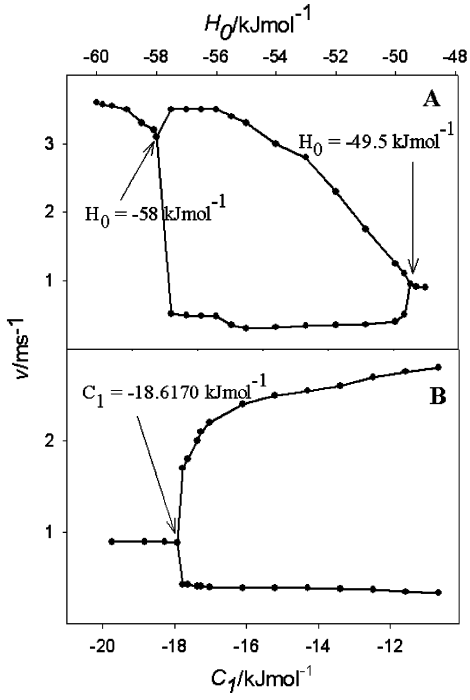

Figure 7. Wave velocity as a function of H_0 (Figure 7A) and C_1 (Figure 7B).

Figure 8. Temperature profile along the pellet for the reference case R. The system, oscillatory along the longitudinal axis, does not show transversal instabilities in the *xy* plane.

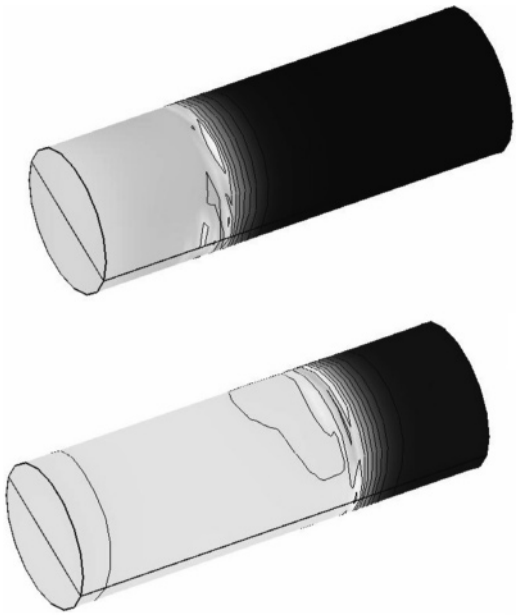

Figure 9. Temperature front along the pellet: transversal instabilities in the *xy* plane can be seen for the longitudinally steady system A2.

are related to the change of mixing enthalpy. In both cases, the system moves toward steady propagation while the exothermicity increased.

The propagation mode is better seen by looking at propagation velocity as a function of time. Considering Figure 5, the system appears to be, in the reference case R, strongly oscillatory with maximum and minimum values well detached one from the other. As the mixing enthalpy changes (column B) and the system becomes more exothermic, the oscillations become narrower but more frequent (plot B1), till reaching a stationary propagation for much higher reaction enthalpies (plot B2). Wave velocity read, when the system becomes stationary, corresponds to an intermediate value between maxima and minima previously observed and is about $\approx$0.9 m s^{-1}.

As the enthalpy of formation of the compound changes (plots A1 and A2), a first stationary profile for the least exothermic system with low propagation velocity (0.85 m s^{-1}) can on the contrary be observed. Colder systems are not able to propagate and directly move toward extinction. Plot A1 shows remarkable similarities with the propagation regime observed in plot B2. In both cases the wave speed is $\approx$0.9 m s^{-1} though a longer transient can be observed in plot B2. Different oscillating situations may be observed while the heat of formation of the compound increases till a last stationary situation with much higher velocity (3.5 m s^{-1}) is reached (plot A2). In this case, the system has an oscillating transient but is afterward able to reach a constant value of propagation velocity. A deeper insight of dynamic behaviors of the system with changing H_0 only can be found in our previous work[16] where the movement of the system along the line A1−R−A2 has been studied with particular attention to initial transients of the system and onset of oscillations.

The overall picture of the dynamics of this SHS reaction as a function of the two parameters H_0 and C_1 is given in Figure 6. Black squares indicate oscillating propagation modes, white squares show steady propagation, and dashes stand for systems that directly encounter extinction.

The values of propagation speed as a function of these two parameters are on the contrary reported in Figure 7. In plots 7A steady propagation modes are met both for most exothermic system (-60 kJ mol^{-1} < H_0 < -58 kJ mol^{-1}) and for the least exothermic case ($H_0 = -49$ kJ mol^{-1}), whereas maximum and minimum values are reported for oscillating systems. In plots 7B unique steady systems can be found for the most exothermic cases (-20.617 kJ mol^{-1} < C_1 < -18.617 kJ mol^{-1}), whereas all other systems show oscillating behavior.

As already said, a 3D model was implemented in addition to the 1D model to study a possible onset of transversal instabilities. Literature reports[17] in fact the existence of such dynamic behaviors in system with longitudinal steady propagation mode. Some previous results concerning the new 3D approach were introduced in a previous work,[16] whereas here a wider scenario can be given. Figures 8 and 9 show temperature profiles along the pellet for the reference case R (Figure 8) and for the "hottest" system considered while the formation enthalpy of the compound is varied (A2). For the reference situation, with oscillations along the *z* axis, no instabilities in the *xy* plane can be outlined. The other system, on the contrary (Figure 9), after an oscillating transient reaches steady longitudinal propagation (plot A2 in Figure 5). The temperature profile along the plane shows on the contrary marked instabilities. In this case two different time steps are shown (Figure 9A,B) for a better demonstration of the persistence of instabilities in the plane. Though not reported in detail, Figure 8 is representative of all systems reported with black dots in Figure 6, and Figure 9 is representative of all systems indicated with white dots. In other words, transversal instabilities appear only in longitudinally steady systems and it appears clear that the fields of existence of these two instabilities appear to be mutually exclusive. Moreover, our reference situation R seems to be a "limit case" in terms of exothermicity, being one of the coldest ones both in terms of H_0 and C_1.

The mechanistic aspects are best clarified for the different cases either by looking at the amounts of the various phases near the reaction front (Figure 10) or by considering the reaction path travelled by the system (Figure 11).

In Figure 10 the continuous line represents the amount of solid compound (normalized to one), the dashed line the composition of the liquid phase, the dotted line the amount of solid aluminum, and the large dashed line the amount of solid Ni. Temperature (right axis) is represented by the dash−dotted line.

It is worth noting that a regular trend of the temperature profile indicates that the two heat release processes occur almost concurrently (A1, A2), or that only one process is active at the reaction front (B2), whereas the presence of knees denotes that different heat release processes occur more separate in space (R, B1). Case B2 is very peculiar in this respect, as the SHS is sustained only by the heat of mixing in the liquid phase, whereas compound formation takes place only in the leftmost part of

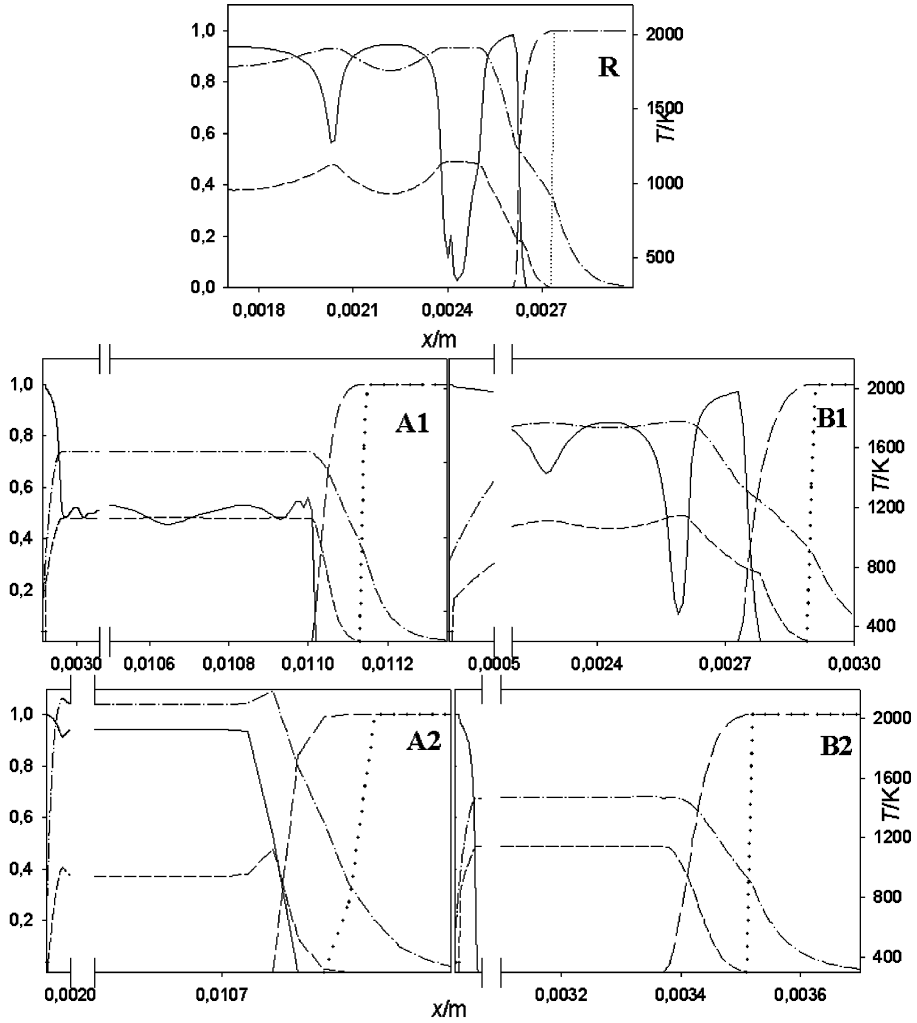

Figure 10. Space profiles, along the reactions front of solid compound (continuous line, left axis), composition of the liquid-phase (short-dashed line, left axis), solid nickel (long-dashed line, left axis), solid aluminum (dotted line, left axis) and temperature (dash−dotted line, right axis). Column B refers to the variation of mixing enthalpy of the liquid phase and column A to the variation of heat of formation of the solid compound. R is the reference case.

the pellet as an afterburn effect far from the leading edge of the thermal wave.

Figure 11 reports the liquidus boundary as a continuous line, and the dots indicate the liquid composition as a function of temperature at different times for a selected point of the sample. This can be considered as a sort of "reaction path" travelled by the system. To analyze these plots, it is important to remember that changing the enthalpy parameters also changes the adiabatic temperature of the system, which in different cases falls well inside the temperature range of the liquidus or is very close to its upper limit. Also in this case, a regular trend of the reaction path indicates predominance of a single heat release process (B2), or almost concurrent activity of the two processes (A1, A2), whereas a knee denotes that different heat release processes occur more separately in time (R, B1).

As a final comment, we note that cases A1 and B2 despite the different nature of the predominant heat release process, show very similar dynamic behavior either concerning propagation mode or wave velocity (in both cases close to 0.9 m s^{-1}).

4. Conclusions

A complete diagram of different propagation modes for the SHS of intermetallic compounds from pure elements was drawn, while two exothermicity parameters were changed: heat of formation of the compound (H_0) and enthalpy of mixing (C_1) but leaving unmodified all kinetic transport parameters (diffusion coefficient and thermal conductivity).

While H_0 and C_1 change, the system encounters: (a) extinction, (b) longitudinally steady propagation, and (c) longitudinally unsteady (1T-pulsed) propagation. Both macrokinetics (wave propagation mode and velocity) and microkinetics (amount of reactants and products in various phases) were analyzed, obtaining a deeper understanding of the leading processes in the SHS of intermetallic compounds.

The pulsed propagation mode appears in the central region of the parameters space and is almost completely surrounded by the steady propagation mode. An abrupt transition was found both between steady propagation and extinction and between pulsed propagation and extinction. This kind of behavior markedly differs from the multiplicity of period doubling cases from unsteady propagation to extinction previously reported in the literature[7,8] and already found by the authors for SHS $Zr + O_2 \rightarrow ZrO_2$. As already pointed out in a former work,[13] there is seemingly a "stabilizing effect" of phase transitions: the constraints due to the phase diagram (even when the phase transitions are not all accounted with an explicit kinetic law) strongly simplify the scenario of propagation modes to be seen.

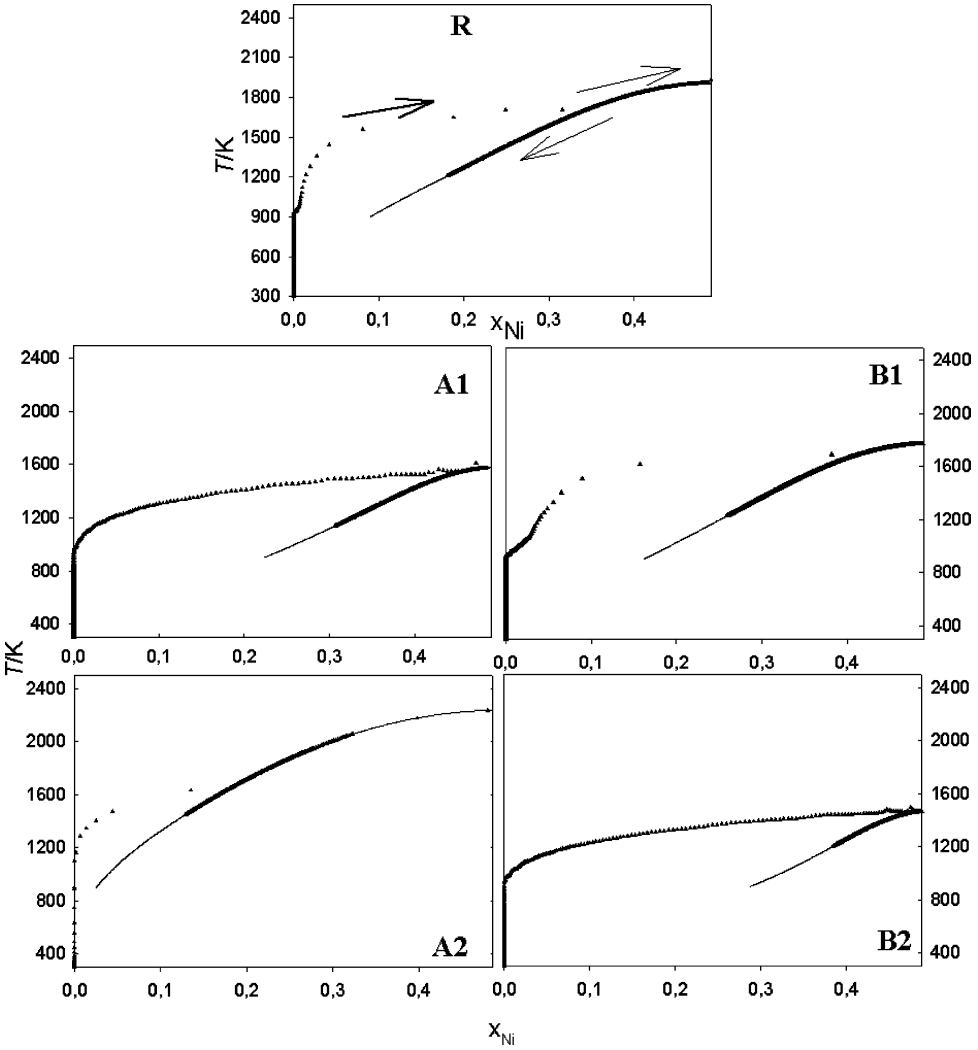

Figure 11. Reaction paths (dots) along the phase diagram (continuous line) while the mixing enthalpy of the liquid phase (B) and heat of formation of the solid compound (A) change.

The SHS can be sustained both by dissolution of high melting metal into the molten pool and by precipitation of the compound; in some cases these two processes take place concurrently, but there are also situations in which they are more or less detached and wave propagation can be sustained only by dissolution of high melting metal.

The 3D simulations show that transversal and longitudinal instabilities have mutually exclusive fields of existence.

References and Notes

(1) Munir, Z. A.; Anselmi-Tamburini, U. *Mater. Sci. Rep.* **1989**, *3*, 277.

(2) Munir, Z. A.; Odink, D. In *Metallurgical Processes of the Early Twenty-First Century*; Sohn, H. Y., Ed.; TMS: Warrendale, PA, 1994; p 167.

(3) Anselmi-Tamburini, U.; Maglia, F.; Spinolo, G.; Munir, Z. A. *J. Mater. Res.* **2000**, *15*, 572.

(4) Boldyrev, V. V.; Aleksandrov, V. V.; Corchagin, M. A.; Tolochko, S. N.; Gusenko, S. N.; Sokolov, A. S.; Sheromov, M. A.; Lyakhov, N. Z. *Dokl. Akad. Nauk SSSR* **1981**, *259*, 1127.

(5) Rogachev, A. S.; Khomenko, I. O.; Varma, A.; Merzhanov, A. G.; Ponomarev, V. I. *Int. J. Self-Propag. High-Temp. Synth.* **1994**, *3*, 239.

(6) Bernard, F.; Gaffet, E.; Gramond, M.; Gailhanou, M.; Gachon, J. C. *J. Synchrotron Radiat.* **2000**, *7*, 27.

(7) Bayliss A., Matkowsky B. J. *SIAM J. Appl. Math.* **1990**, *50*, 437.

(8) Bayliss A., Matkowsky B. J. *SIAM J. Appl. Math.* **1994**, *54*, 147.

(9) Weber, R. O., Mercer, G. N.; Sidhu, H. S.; Gray, B. F. *Proc. R. Soc. London A* **1997**, *453*, 1105.

(10) Weber, R. O., Mercer, G. N., Sidhu, H. S. *Proc. R. Soc. London A* **1998**, *454*, 2015.

(11) Arimondi, M.; Anselmi-Tamburini, U.; Gobetti, A.; Munir, Z. A.; Spinolo, G. *J. Phys. Chem. B* **1997**, *101*, 8059.

(12) Maglia, F.; Anselmi-Tamburini, U.; Gennari, S.; Spinolo, G. *Phys. Chem. Chem. Phys.* **2001**, *3*, 489.

(13) Maglia, F.; Anselmi-Tamburini, U.; Gennari, S.; Spinolo, G. *J. Phys. Chem. B* **2002**, *106*, 6121.

(14) Gennari, S.; Maglia, F.; Anselmi-Tamburini, U.; Spinolo, G. *J. Phys. Chem. B* **2003**, *107*, 732.

(15) Gennari, S.; Maglia, F.; Anselmi-Tamburini, U.; Spinolo, G. *Intermetallics* **2003**, *11*, 1355.

(16) Gennari, S.; Maglia, F.; Anselmi-Tamburini, U.; Spinolo, G. Manuscript submitted.

(17) Makino, A. *Prog. Energ. Combust.* **2001**, *27*, 1.

(18) Murray, J.; Peruzzi, A.; Abriata, J. P. *J. Phase Equilib.* **1992**, *13*, 277.

(19) Hansen, M.; Anderko, K. In *Metallurgy and Metallurgical Engineering Series: Constitution of Binary Alloys*; Mehl, R. F., Bever, M. B. Eds.; MacGraw-Hill Book Co.: New York, Toronto, London, 1958.

(20) Grigorovitch, K. V.; Krylov, A. S. *Thermochim. Acta* **1998**, *314*, 255.

(21) Programme CFD-ACE(U), CFD Research Co., Huntsville, AL.

(22) Gennari, S. Ph.D. Thesis, University of Pavia, 2003 (in Italian).

(23) Aaron, H. B.; Fainstein, D.; Kotler, G. B. *J. Appl. Phys.* **1970**, *41*, 4404.

(24) Milanese, C. Ph.D. Thesis, University di Pavia, 2001 (in Italian).